Alignment-controlled O_2 chemisorption and catalytic CO oxidation on curved Pt(111)

Mitsunori Kurahashi*

National Institute for Materials Science, 1-2-1 Sengen, Tsukuba, 305-0047, Japan

E-mail: kurahashi.mitsunori@nims.go.jp

Abstract

Steric effects in O_2 chemisorption and catalytic CO oxidation on stepped Pt(111) surfaces have been investigated by scanning a narrow alignment-controlled O_2 beam across a curved Pt(111) surface, on which the densities of {100} (A-type) and {111} (B-type) steps vary smoothly with the distance from the center of the crystal. The contribution of trapping-mediated and activated chemisorption to these processes on the terraces and steps were discussed based on the dependence of these processes on the kinetic energy (80-500 meV) and alignment of O_2. The results indicate that (i)the probability of activated O_2 chemisorption on surfaces with type-B steps is slightly lower than that on surfaces with type-A steps, (ii) CO oxidation proceeds both at terraces and steps at the sample temperature of 693 K while it happens only at terraces at 423 K. The results of CO oxidation experiments at 423 K indicate that the rate of CO_2 production at terraces of the stepped Pt(111) surface is lower than at a flat (111) surface and depends on the step structure.

Introduction

O_2 adsorption and CO oxidation on platinum (Pt) have been investigated intensively due to their relevance to technologically important catalytic processes such as the O_2 reduction reaction in fuel cell and car exhaust gas purification. Since steps are considered to play key roles in these reactions on nanoparticle catalysts, much effort has been made to clarify the mechanism of these processes on stepped Pt using vicinal single-crystalline surfaces as model systems.[1] A cylindrical crystal where the step density varies smoothly on the surface,[2,3] or a curved crystal, which is a part of the cylindrical single crystal,[4–12] have also been employed since scanning the analysis point on the surface allows us to investigate the step density and structure dependence of the reactivity under the same experimental conditions. Studies using this methodology have also clarified the subtle effects of steps on the properties of adjacent terraces, which may be difficult to observe with the use of high-index single-crystal surfaces.

For instance, the combined use of high-resolution X-ray photoemission spectroscopy (XPS) and a curved Pt(111) crystal has shown that the electronic properties of microterraces in stepped surfaces are not identical to those of a flat surface, which can be attributed to the strain induced by the step.[8] The effects of the step structure on the temperature dependence of CO oxidation together with the XPS characterization of the chemical species existing on the surface under millibar pressure have been investigated using Pt,[4] Rh[5] and Pd(111)[6,7,13] curved crystals.

On the other hand, the mechanism of gas-surface reactions depends on the kinetic energy, orientation, and internal state of gas-phase molecules that collide with the surface. Molecular beams with well-defined initial states have been used to clarify this.[14,15] Regarding the O_2/Pt(111) system, previous studies have shown that O_2 dissociates via molecular chemisorption followed by thermal dissociation, and that two basic mechanisms exist for O_2 molecular chemisorption.[16] One is the trapping-mediated process where O_2 is initially trapped into the physisorbed state and then thermally activated to the chemisorbed state. The other is the chemisorption activated by the kinetic energy of impinging O_2. The contributions of these two processes mix in reaction experiments with thermal gases. Non-state-resolved O_2 molecular beam studies on high index surfaces[17] and curved crystal surfaces[11] have shown that steps enhance the probability of trapping-mediated chemisorption, while the probabilities of activated chemisorption at the steps and terraces are not largely different. State-resolved O_2 beam studies on flat[18] and high-index surfaces[11,19] have shown that the probability of activated chemisorption depends strongly on the O_2 alignment relative to the surface local structure while the trapping-mediated process does not. Considering the fact that the strain induced by the step affects the electronic properties of terraces as demonstrated by previous XPS/curved crystal studies,[8] it might be reasonable to expect that the step also affects alignment-dependent O_2 chemisorption and the subsequent catalytic reactions on the adjacent terrace. However, no attempts have been made to investigate this issue.

In the present study, we have studied alignment-dependent O_2 chemisorption and cat-

alytic CO oxidation on a curved Pt(111) surface. A narrow state-selected O_2 beam was scanned across a curved crystal to investigate the step density and O_2 alignment dependence of these processes. Although the overall behavior of the O_2 sticking probability can be understood based on the results of previous studies on flat and stepped Pt(111) surfaces, the results show that O_2 sticking probabilities on the terrace of the stepped Pt(111) are not identical with those on a flat (111) surface. The step density dependence of the CO oxidation rate indicates that the low-temperature CO oxidation proceeds only at the terrace of the stepped surface. Using this fact, we will discuss the difference in the reactivity between a terrace of the stepped Pt and a flat (111) surface.

Experiments

The experiments were conducted with a single spin-rotational state-selected [(J,M) =(2,2)] O_2 beam prepared by combining a supersonic seeded O_2/He beam with a hexapole magnet.[20–22] The translational energy (E_0) of the state-selected O_2 beam was varied within a range of 0.08-0.5 eV by adjusting the length of the hexapole and tuning the velocity of the supersonic seeded O_2 beam. The O_2 internuclear axis is mainly perpendicular to the defining magnetic field (H_{def}) while its electron spin is oriented parallel to the magnetic field in this state.[20,21] There are three non-equivalent geometries on a non-magnetic stepped Pt(111) surface [Fig. 1(a)]. The O_2 axis is mainly parallel to the (111) terrace [helicopter geometry (H)] when H_{def}// [111], while parallel and perpendicular O_2 are distributed equally (cartwheel geometry) when H_{def} is parallel to the (111) terrace. Two non-equivalent cartwheel geometries exist. The O_2 axis is perpendicular to the step direction if H_{def}//$[1\bar{1}0]$ [C_Z in Fig. 1(a)] while it is parallel to the step (C_Y) if H_{def} // $[\bar{1}\bar{1}2]$. A comparison of the reactivities in the C_Y and C_Z geometries permits the discussion of the alignment effect relative to the step direction.[11] In this study, however, since we focused our attention to the alignment effect in O_2 chemisorption on the terrace of the stepped Pt surfaces, only the difference in the O_2

sticking probability and CO oxidation between the H and C_Z geometries will be presented.

The molecular beam apparatus is connected to an analysis chamber where the O_2 sticking and surface reaction experiments are conducted. A slit with an opening of $\sim$0.2×2 mm was used as the final aperture of the beamline to prepare a narrow aligned O_2 beam. The O_2 sticking probability was measured at normal incidence to the (111) terrace and at a sample temperature of 313 K using the King and Wells (KW) method[23] with an ion gauge (IG). The KW traces at about 10 different points on the surface were taken at one time for a cleaned curved Pt(111) surface by scanning the sample position with a stepping motor. Since the O_2 pressure in the analysis chamber during the KW measurement was $< 2\times10^{-10}$ Torr and the beam irradiation time for taking one KW trace was $\sim$20 seconds, the exposure to the background O_2 gas while taking the ten KW traces is estimated to be < 0.04 Langmuirs. The percentage of O_2 in the primary beam that passes through the final aperture was found to be nearly 100% from the gas analysis during the beam irradiation. This comes from the fact that the magnetic hexapole focuses only O_2 and the center stop located in the beamline removes most of the He atoms contained in the He-seeded O_2 beam.[21] Isotopically labelled ^{13}CO used for monitoring the catalytic CO oxidation reaction on the surface was introduced to the analysis chamber using a gas doser to obtain higher local CO pressures at the sample position. H_{def} of about 1 Gauss was applied to the sample region using 3 pairs of Helmholtz coils for controlling the O_2 alignment. No difference was found in the IG signal between the H and C_Z geometries when the O_2 beam was scattered by an inert flag, which was positioned in front of the surface, indicating that the direction of the applied magnetic field does not affect the flux of the O_2 beam. An example of this measurement is shown in Fig. 10 in Ref. [21]. Here, the vacuum vessels that house the ion sources of the IG and the residual gas analyzer (RGA) were magnetically shielded with permalloy plates to prevent the effects of the magnetic field change on their signals during the alignment-controlled experiments.

We used a polished curved Pt(111) crystal obtained from Surface Preparation Laboratory, the Netherlands. It is a 31° section of a 30 mm diameter cylinder and the surface provides a

continuous range of substrates, from a flat Pt(111) surface up to vicinal angles (α) of $\pm$15.5 ° [Fig. 1(a)]. Steps are along the close-packed [1$\bar{1}$0] direction and α varies along the [$\bar{1}\bar{1}$2] direction. The (111) terraces of the vicinal surfaces are separated by {100} like steps, which are denoted as A-type steps, in the [$\bar{1}\bar{1}$2] direction and by {111}-like steps, which are denoted as B-type steps, in the [11$\bar{2}$] direction. The crystal surface was cleaned in a preparation chamber, which is connected to the analysis chamber mentioned above, by repeating 1 kV Ar^+ sputtering at 823 K, oxidation at 823 K under the O_2 pressure of 1×10^{-8} Torr, and annealing at 1023 K. The final annealing process before reaction experiments was conducted at 823 K since a previous study showed that the low-temperature annealing prevents the restructuring and faceting of the vicinal surfaces.[9] The preparation chamber is equipped with a low energy electron diffraction (LEED) optics and a cylindrical mirror analyzer for Auger electron spectroscopy (AES) measurements. The LEED pattern of the surface showed sharp spots from the vicinal surface [Fig. 1(b)]. The spot separation, which is known to be nearly proportional to the terrace width,[24] varied smoothly with the distance from the crystal center (y), indicating smooth terrace-width variation on the surface. No impurity was found within the detection limit of the AES measurements.

Results

O_2 sticking probability

Figure 2(a) shows the initial sticking probability (S_0) of O_2 for the helicopter (H) and cartwheel (C_Z) geometries measured at different positions (y) on the curved Pt(111) crystal. Different panels correspond to the results taken at different O_2 kinetic energies. Here, the position y=0 corresponds to the flat surface, and the A- and B-type steps are distributed at y<0 and y>0, respectively. Figure 2(b) shows the sticking probability difference between the two geometries [ΔS_0=$S_0(H)$-$S_0(C_Z)$]. Contributions of the trapping-mediated process, which is dominant at low E_0 and shows no alignment dependence, and the activated O_2

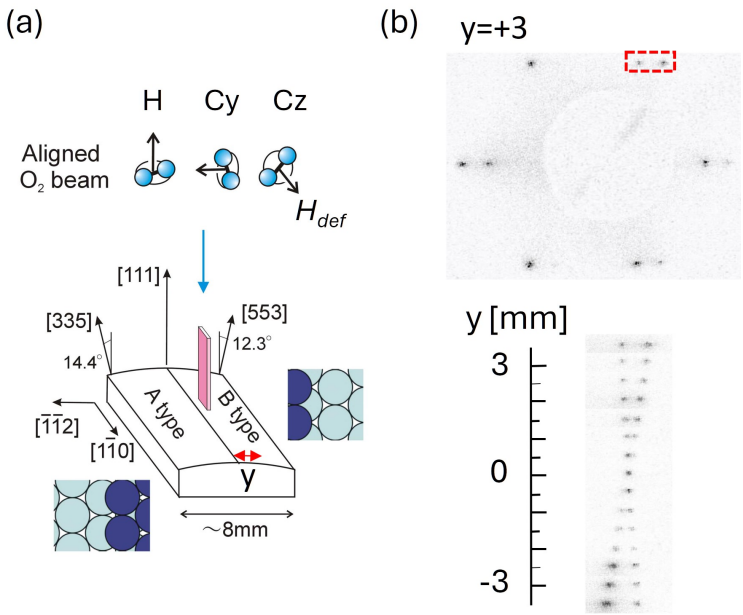

Figure 1: (a) Three non-equivalent geometries for O_2 molecules in the (J,M)=(2,2) state and the structure of the curved Pt(111) crystal used in this study. Coordinate y is taken along the $[11\bar{2}]$ direction and is graduated from the center of the crystal. {100}- and {111}-like steps exist at the y<0 and y>0 sides, respectively. (b) LEED pattern of the curved Pt(111) surface taken at y=+3 mm with beam energy of 225 eV. The position dependence of the LEED spots indicated by the red dashed rectangle in the upper panel is shown below.

chemisorption, which is dominant at high E_0 and shows a large alignment dependence, need to be considered to discuss these results.

The S_0 and ΔS_0 values show the following behaviors at the lowest energy (E_0=76 meV). The first panel of Fig. 2(a) shows that S_0 increases linearly with the distance from the crystal center ($|y|$) while the slope of the increase is larger for the B-type step side. This can be understood based on the previous studies on (553) and (335) surfaces,[11,17] which have shown that steps enhance precursor-mediated chemisorption and the efficiency is higher for the type-B step. The linear increase of S_0 with $|y|$ can therefore be attributed to the increase of the probability of the precursor-mediated process with increasing the step density. In contrast, as shown in Fig. 2(b), ΔS_0 is largest at the flat surface (y=0) and decreases largely with increasing $|y|$. Here, ΔS_0 is associated with the activated process, which happens both at terraces and steps. To discuss the y dependence of S_0 and ΔS_0, we need to consider the percentage of terrace and step areas within the stepped surface as well as the reactivity of these areas. The (553) plane, which has a five atom wide terrace, is positioned at y=+3.2 mm of the present curved Pt(111) crystal. Although the geometric percentage of the terrace area in the (553) plane is about 60% as will be discussed later, the ΔS_0 value at y$\sim$+3 mm is shown to be less than 30 % of the value at y=0.

With increasing E_0, the y dependence of S_0 becomes more gradual while the alignment dependence in S_0 becomes more clear. This reflects the dominance of the activated process at higher E_0. As to the alignment effect, Fig. 2(b) shows that the y dependence of ΔS_0 becomes weaker with increasing E_0. It is noted that, at $E_0 > 200$ meV, the S_0 values on the type-B step side are a little lower than those on the type-A step side. The lower S_0 on the type-B step side was not observed in the previous non-state-resolved O_2 chemisorption study on curved Pt(111).[11] This might be because the measurement was conducted at 150 K and with a relatively low beam energy ($E_0<$ 260 meV),[11] where the contribution of the trapping-mediated process may be larger than the present case.

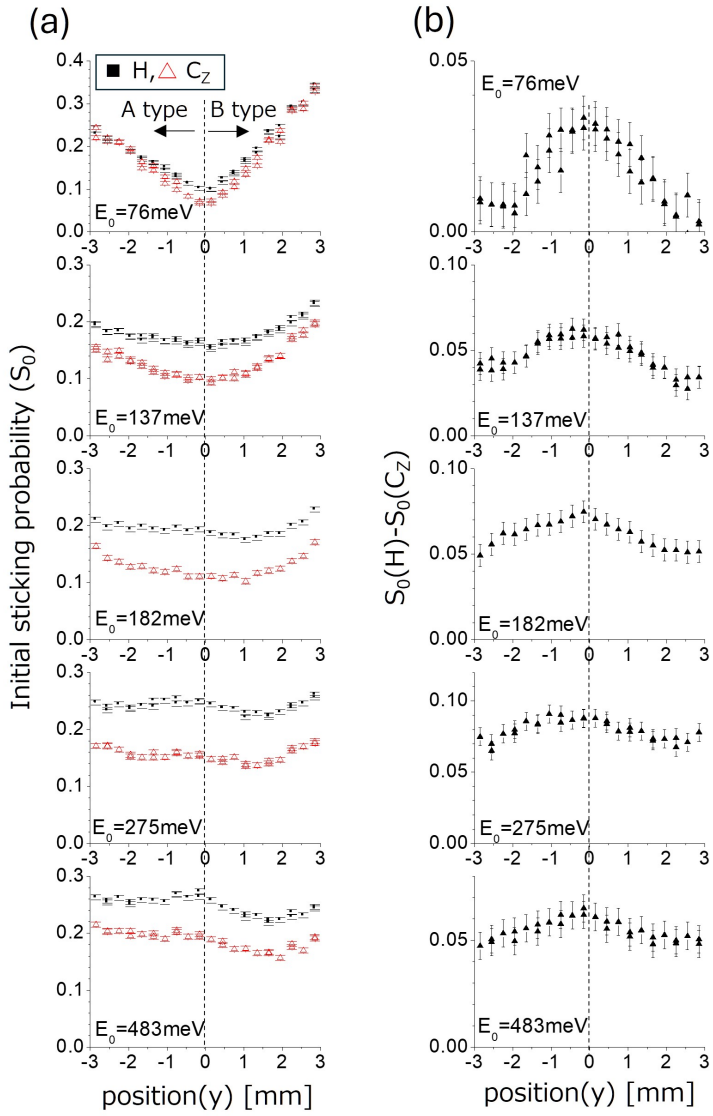

Figure 2: (a)The initial sticking probability (S_0) of O_2 for helicopter (H) and cartwheel (C_Z) geometries measured as a function of the position (y) on the Pt(111) curved crystal and (b) the difference in S_0 between the two geometries. Different panels correspond to the results for the O_2 kinetic energies shown. Error bars were derived from the fluctuation of the ion gauge signals used for deriving the S_0 values.

CO oxidation

Temperature dependence of CO oxidation at low O_2 kinetic energy

Figure 3 shows the time evolution of the steady-state CO oxidation reaction measured while the aligned O_2 beam with E_0=76 meV irradiates the curved Pt(111) surface under a background CO pressure of 3×10^{-7} Torr. The three profiles correspond to those measured at sample temperatures (T_S) of (a)593 K, (b)523 K and (c)423 K. The CO_2 production rate was monitored with the RGA at the position (y) on the sample shown in Fig. 3(a). The beam irradiation (about 160 sec.) and the movement to the next position with the O_2 beam off were repeated. The H and C_Z geometries of O_2 were alternated every 20 seconds during irradiation. The H geometry resulted in higher CO_2 production rates than the C_Z geometry due to the higher O_2 sticking probability for the helicopter geometry. The behavior observed at $y\sim0$ is similar to that for the O_2 alignment-controlled CO oxidation on a flat Pt(111).[25] The O_2 pressure equivalent to the flux of the O_2 beam used for measuring the profiles shown in Fig. 3 was roughly estimated to be 3.4×10^{-6} Torr from the O_2 pressure in the analysis chamber during the beam irradiation, the nominal pumping speed of the turbomolecular pump and the beam size on the sample. In the present experiment, CO gas was initially introduced to the analysis chamber, and O_2 beam irradiation followed. It is known that CO oxidation does not occur if the surface is completely covered with CO, but CO oxidation happens above 305 K on a flat Pt(111) surface since some CO molecules desorb above this temperature.[26] It would be because the sample temperature employed in this study was $>$ 305 K that the steady-state CO oxidation reaction was observed.

The profile for the CO_2 production rate at 593 K [Fig. 3(a)] exhibits a minimum at $y\sim0$ and increases with increasing distance from the crystal center ($|y|$) while the CO_2 yields at $y> 0$ is shown to be higher than at $y< 0$. These results indicate that CO oxidation happens both at the terrace and step at 593 K. The behaviors are consistent with the fact that S_0 increases with increasing $|y|$ at E_0=76 meV and S_0 is higher on the type-B step side [Fig.

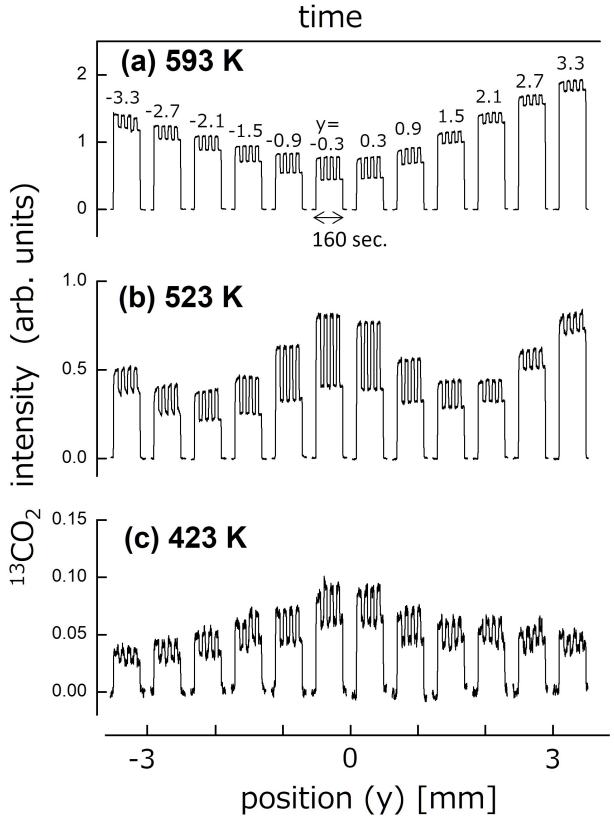

Figure 3: Time evolution of the CO_2 production rate measured during O_2 beam irradiation (E_0=76 meV) on a curved Pt(111) crystal at T_S of (a) 593 K, (b) 523 K and (c)423 K under the background CO pressure (P_{CO}=3 x 10^{-7} torr). The reaction measurement at the position (y) shown in the figure and the movement to the next position with the O_2 beam off was repeated. The H and C_Z geometries of O_2 were alternated during measurement. The H geometry resulted in higher CO_2 production rates.

2(a)]. The difference in the CO_2 yield between the H and C_Z geometries is largest for the flat surface and decreases with increasing $|y|$. This is also consistent with the decrease of ΔS_0 with increasing $|y|$ [Fig. 2(b)]. The similarity of the y dependence of the CO_2 yield at 593 K and the O_2 sticking probability at the clean Pt surface suggests that the rate constant of CO oxidation at 593 K is similar between the step and the terrace at this CO pressure condition.

Figures 3(a)-(c) show that the CO_2 production rate changes significantly with temperature at around 523 K while the threshold temperature, so-called ignition temperature, depends on the step density. At $y\sim0$, the CO_2 yield at 423 K is about 10% of that at 593 K while the yields at 523 K and 593 K are similar. This is consistent with previous studies showing that the CO_2 production rate on a flat Pt(111) surface increases drastically at 500-550 K with increasing temperature and changes gradually at higher temperatures.[2,4,27] Therefore, we judged that the CO oxidation rate at the flat surface region is saturated at 593 K, although experiments at higher temperatures were not conducted. In contrast, at $y\sim\pm3$ where the step density is high, the CO_2 yield at 523 K is 30-50% of that at 593 K. The profile at 423 K [Fig. 3(c)] shows that the CO_2 yield is highest at $y\sim0$ and decreases monotonically with increasing $|y|$. These behaviors indicate that the low-temperature CO oxidation is inefficient at steps and the profile at 423 K virtually reflects the reactions at the terrace of the stepped surface. A previous thermal desorption study[28] on Pt(335) has shown that the binding energy of CO at the step site is higher than that at the terrace site. Oxidation of CO molecules adsorbed at steps would, therefore, require higher sample temperatures, causing the inefficient low-temperature CO oxidation at steps. In the present experiment, since the surface was initially exposed to the background CO gas, step sites would be blocked by strongly bound CO molecules and would not contribute to the CO oxidation reaction at 423 K.

It is possible that the CO oxidation changes the atomic arrangement at the step since there have been experimental evidences showing that O_2 chemisorption induces the step

doubling of transition metal surfaces.[29,30] The structural analysis with LEED at the position of the O_2 beam irradiation was not conducted in this study. However, Fig. 3(a) shows that the CO_2 yield varies smoothly with the distance from the crystal center at 593 K, suggesting that the step density of the clean surface would not be changed largely in the present conditions.

Low-temperature CO oxidation at high O_2 kinetic energy

Figure 4(a) shows the CO oxidation profile measured with the aligned O_2 beam of E_0=275 meV at 423 K. Since trapping-mediated O_2 chemisorption is inefficient at this energy[11,16–18] and steps do not contribute to CO oxidation at 423 K as shown above, these profiles reflect CO oxidation caused by the activated O_2 chemisorption at terraces of the stepped Pt. The three panels correspond to the profiles at different relative CO pressures.

We first discuss the CO pressure dependence of the profile at $y\sim0$. Figure 4(a) shows that the ratio of the CO_2 intensity for the helicopter geometry [I(H)] to that for the cartwheel geometry [I(C_Z)] is about 1.4 at P(CO)/P^e(O_2) =0.15 [the top panel of Fig. 4(a)] while it increases to $\sim$1.8 at P(CO)/P^e(O_2)$>$ 0.3. On the other hand, Fig. 2(a) indicates that the sticking probability ratio between the H and C_Z geometries [$S_0(H)/S_0(C_Z)$] at E_0=275 meV and at $y\sim$ 0 is $\sim$ 1.7, which is similar to the value of I(H)/I(C_Z) at P(CO)/P^e(O_2)$>$ 0.3. This can be understood as follows. CO oxidation on Pt proceeds via the Langmuir-Hinshelwood mechanism, in which O_2 chemisorption followed by a reaction of adsorbed O and CO forms CO_2.[27] The CO_2 production rate would be proportional to the product of the concentrations of CO and atomic O on the surface. In the steady-state reaction, the CO concentration is determined by competition between CO adsorption from the gas phase and its consumption for CO_2 production. Because the sticking probability of helicopter O_2 [S(H)] is higher than that for cartwheel O_2 [S(C_Z)], the CO concentration during the steady-state reaction for helicopter O_2 would be lower because more CO molecules are consumed for CO_2 production. This would result in I(H)/I(C_Z) $<$ S(H)/S(C_Z). However, if the CO pressure is

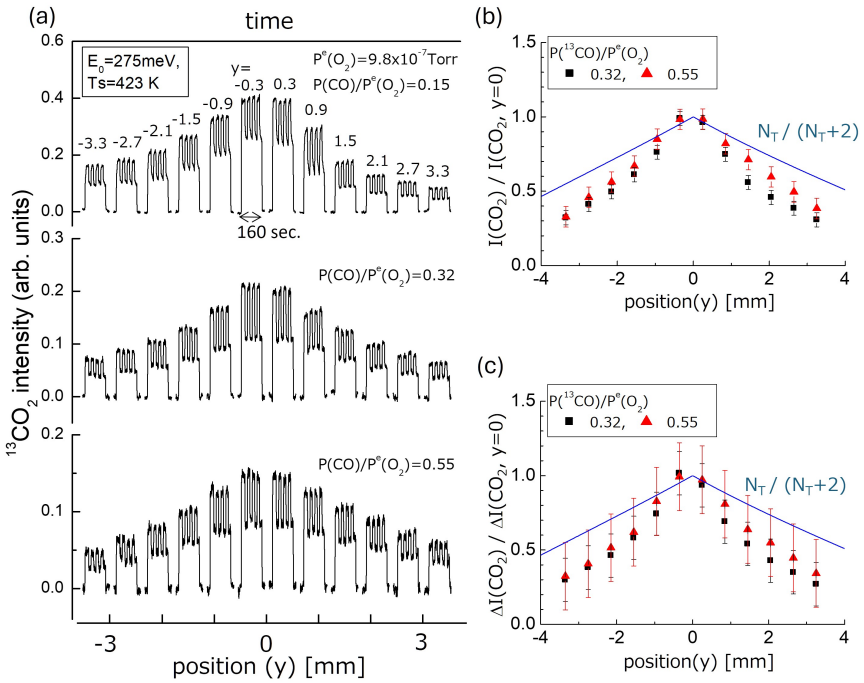

Figure 4: (a) Time evolution of the CO_2 production rate measured while the O_2 beam with E_0=275 meV irradiates the position (y) on the curved Pt(111) at T_S=423 K. The H and C_Z geometries of O_2 were alternated during measurement. The three panels correspond to the results taken under different background CO pressures. The ratio between the background CO pressure and the O_2 pressure equivalent with the beam flux [$P^e(O_2)$] is shown. (b)The position dependence of the CO_2 production rate at the helicopter geometry normalized by the value at y=0. The ratio of the terrace atoms within the surface is shown with solid blue lines. (c)The position dependence of the difference in the CO_2 production rate between the H and C_Z geometries normalized by the value at y=0. Error bars shown in (b) and (c) were estimated from fluctuations in the CO_2 signal.

high enough to cause the CO adsorption rate $\gg$ the O_2 sticking probability, the CO coverage during the reaction for the two geometries would be similar. In such conditions, the CO_2 production rate is expected to be proportional to the O_2 sticking probability.

We secondly discuss the CO oxidation at stepped surfaces. The profile at $P(CO)/P^e(O_2)$ = 0.15 shows that the ratio $I(H)/I(C_Z)$ increases with increasing $|y|$. For example, this ratio is $\sim$1.4 at y=-0.3 while it is $\sim$1.8 at y=2.7. If the reactivity of the microterrace of the stepped surface is identical with that of the flat surface, $I(H)/I(C_Z)$ for the microterrace should be identical to that for the flat surface. In addition, the profiles on the A- and B-type step sides are not symmetrical. It is shown that the CO_2 yield is lower and $I(H)/I(C_Z)$ is higher on the B-type step side. These behaviors may be accounted for if the O_2 sticking probability is lower on the type B step side. The fact that S_0 on the B-stepped surface is slightly lower at E_0=275 meV [Fig. 2(a)] might be associated with this.

Figures 4(b) and (c) summarize the position dependence of the CO_2 yield for the helicopter geometry [$I_{CO_2}(H)$] and the difference between the H and C_Z geometries [ΔI_{CO_2}], respectively. The data taken at high CO pressures where the CO_2 production rate may be proportional to the O_2 chemisorption probability are plotted. These quantities are normalized by the values at y=0, which were estimated by the fit of the data points at -1<y< 1 to parabolic functions. To discuss the contribution of the terrace area to the reactivity of the stepped Pt surfaces, the ratio of the number of terrace atoms (N_T) to the total number of terrace, edge and corner atoms on the surface [n_T=$N_T/(N_T$+2)] is shown with solid blue lines. The data points for $I_{CO_2}(H)$ and ΔI_{CO_2} are expected to be around these lines if the terrace of the stepped surface has the same reactivity with a flat (111) surface and the step gives no contribution to $I_{CO_2}(H)$ and ΔI_{CO_2}. In previous O_2 chemisorption study on Pt(553),[17] $\sim$50% of the surface area was assumed to act like the Pt(111) surface for discussing the contribution of the terrace area to the measured sticking probability. The (553) surface, which has five atom wide terraces (n_T = 0.6), is at y=+3.2mm in the present curved Pt(111) crystal.

Figures 4(b) and (c) show that, unlike S_0 and ΔS_0 at E_0=275 meV [Fig. 2(a)], $\mathrm{I}_{CO_2}(H)$ and $\Delta\mathrm{I}_{CO_2}$ decrease largely with increasing $|y|$. This reflects the following situations. Activated O_2 chemisorption occurs at the terraces and steps and its probability depends on the O_2 alignment. The contribution of the terraces to S_0 and ΔS_0 decreases while that of the steps increases with increasing $|y|$, resulting in the weak position dependence of S_0 and ΔS_0. However, since the low-temperature CO oxidation happens only at the terrace, $\mathrm{I}_{CO_2}(H)$ and $\Delta\mathrm{I}_{CO_2}$ decreases with the decrease of the terrace area. $\mathrm{I}_{CO_2}(H)$ and $\Delta\mathrm{I}_{CO_2}$ show similar profiles, implying that the O_2 alignment effects in CO oxidation at the microterraces and the flat surface are similar. We note that the normalized values for $\mathrm{I}_{CO_2}(H)$ and $\Delta\mathrm{I}_{CO_2}$ are 20-50 % lower than the ratio of the terrace atoms within the surface (solid blue lines).

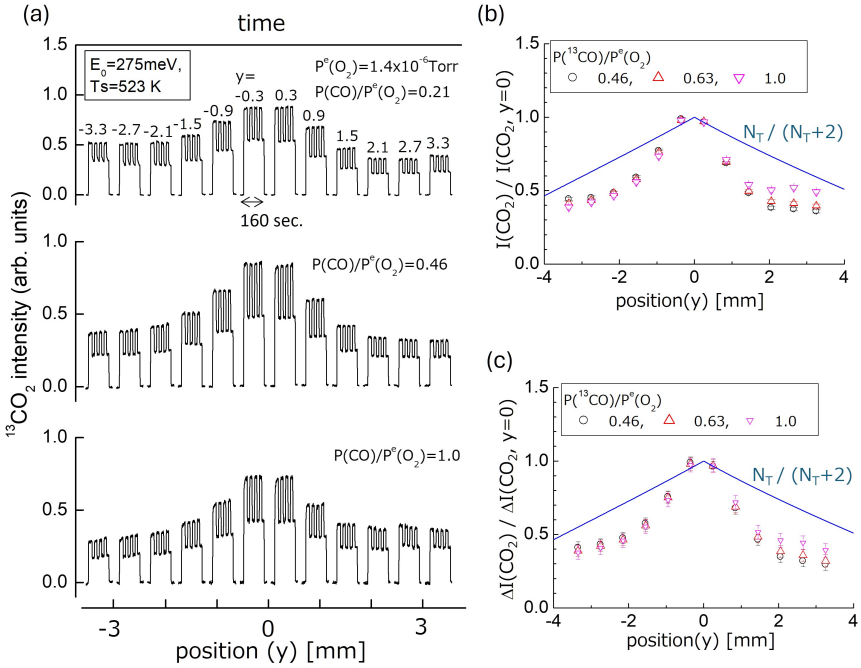

Figure 5: (a) Time evolution of the CO_2 production rate measured while the O_2 beam with E_0=275 meV irradiates the indicated position (y) of the curved Pt(111) crystal at 523 K. The H and C_Z geometries of O_2 were alternated during measurement. The three panels correspond to the results taken under different background CO pressures. The position dependence of (b) the CO_2 production rate at the helicopter geometry and (c) the difference in the CO_2 production rate between the H and C_Z geometries normalized by the value at y=0. Error bars shown in (b) and (c) were estimated from fluctuations in the CO_2 signal.

Figure 5 shows the CO_2 production rate measured at 523 K and E_0=275 meV. As shown

in Fig. 3, this temperature is around the ignition temperature of CO oxidation on the flat surface. It is shown that the CO_2 production rate changes gradually with y at highly stepped regions ($|y| > 2$). This reflects the situation that CO oxidation also happens at steps at 523 K although its efficiency is lower than at the terrace. As to the shape of the profile for the CO_2 production rate at around y=0, it is found from the comparison of Figs. 4(b) and 5(b) that the width of the profile at 523 K is narrower than at 423 K, and that the CO_2 production rate at 523 K decreases more steeply with increasing $|y|$. This cannot be attributed to the effect of the temperature on the O_2 chemisorption step since the activated O_2 chemisorption dominant at this energy is insensitive to T_S. We speculate that the step might affect the ignition temperature of CO oxidation on the adjacent terrace, although additional information is needed for further discussions.

Discussion

The present results indicate that the reactivity of the terrace of the stepped surface is likely to be different from that of the flat surface. The previous XPS study on curved Pt(111) [8] have shown that the Pt 4f level of the terrace surface shifts to the higher binding energy side with increasing the step density. This has been associated with the lattice contraction induced by the step. The contraction of $\sim$2% has been estimated for the terrace of (335) and (553) surfaces while the estimated contraction is slightly larger for the (553) surface with the B-type step. [8] On the other hand, a theoretical study by Mavrikakis at al. predicted that the lattice contraction reduces the adsorption energy of molecules, [31] while the O_2 reduction efficiency on strained Pt films on nanoparticles has been shown to be largely different from that on bulk Pt. [32] Considering the results of these studies, it may be reasonable to expect that the lattice contraction increases the activation energy for molecular chemisorption, reducing the probability of the activated chemisorption of O_2. Fig. 2(b) shows that ΔS_0 decreases largely with the step density at E_0=76 meV. The values at highly stepped regions

can not be explained if we assume that the terrace of the stepped Pt has the same reactivity with a flat Pt(111) surface. For example, the ΔS_0 value at $y{\sim}2$ mm, where the $n(T)$ value shown in Fig. 4 is ~ 0.7, is much less than 0.7 x ΔS_0 (y=0). In addition, Figure 4 shows that $\mathrm{I}_{CO_2}(H)$ and $\Delta\mathrm{I}_{CO_2}$ for the low-temperature CO oxidation on the terrace of stepped Pt are considerably smaller than those expected for the reactivity of a flat Pt(111) surface. These results may be consistent with the lattice contraction induced by the step, which would increase the activation energy for chemisorption at the terrace of the stepped Pt, because, in such cases, the O_2 sticking probability and its alignment dependence would also become smaller.

It is known that S_0 of O_2 on a flat Pt(111) surface is much less than unity (< 0.3) even when the O_2 kinetic energy is increased to $\sim$ 1.0 eV.[16,18] This has been associated with a situation in which, although energetic O_2 molecules can surmount the activation barrier for molecular chemisorption, the probability of being scattered off from the surface by the repulsive wall of the interaction potential increases with increasing E_0.[18] We speculate that, if the lattice contraction increases the activation barrier for O_2 chemisorption, it would also increase the probability of scattering, making the sticking probability of energetic O_2 molecules lower than that on a flat Pt(111) surface. The lower S_0 on the B-step side at high E_0 conditions, which is shown in Fig. 2(a), may be consistent with the theoretical simulation predicting that the lattice contraction induced by the B-type step is larger than that induced by the A-type step.[8]

To discuss the origin of the reduced reactivity of the microterraces, we may also have to consider the effective terrace width. The percentage of the terrace area in stepped surfaces shown in Figs. 4 and 5 was estimated by assigning the edge and corner atoms as the step area. The effective terrace width can be narrower than the width estimated with this assumption because the corner and edge atoms, which have been predicted to be strongly strained,[8] can affect the potential of neighboring area. If, for example, we assign additional 0.5 atom row to the step area, the percentage of the terrace area is reduced to 50% for (553) surface, which is

the value employed by Jacobse et al.[17] To make quantitative discussions as to how much the reactivity of the microterrace is reduced, additional information about the effective terrace width would be necessary.

Figure 3 shows that CO oxidation at low temperature is less efficient at steps than at terraces. This appears inconsistent with the results of the recent near-ambient pressure (NAP)-XPS study[4] of CO oxidation on curved Pt(111), which showed that stepped and flat Pt(111) surfaces have identical ignition temperatures. The NAP-XPS study of CO oxidation on curved Pt(111) was conducted with a CO and O_2 gas mixture at millibar pressures, and the presence of subsurface oxygen on the (111) terrace was suggested to cause the identical ignition temperature. In the present experiment, however, the O_2 beam irradiates the CO-exposed Pt surface where no subsurface oxygen exists. The difference in the reaction conditions between the two experiments might result in the different temperature dependences of CO oxidation.

Conclusion

By scanning a narrow rotational-state-selected O_2 beam on a curved Pt(111) surface where the step density varies smoothly across the crystal, we have investigated the effect of the step on the alignment-dependent O_2 chemisorption and catalytic CO oxidation on vicinal Pt(111) surfaces. To the best of our knowledge, this is the first state-selected molecular beam reaction experiment on a curved crystal surface. It has been shown that this approach helps us to separate contributions of the precursor-mediated and activated processes on terraces and steps in vicinal surfaces. The increase in the probability of trapping-mediated O_2 chemisorption with increasing the step density, its step-type dependence and the dominance of activated chemisorption at high energy conditions were observed and found to be consistent with previous studies on stepped Pt. However, the results show that the probability of activated chemisorption on surfaces with type-B steps is slightly lower than on surfaces with

type -A steps. The step density dependence of the low-temperature (423 K) CO oxidation, which was found to occur only at terraces of stepped Pt surfaces, indicates that the CO_2 production rate at the terraces of the stepped Pt is lower than at a flat (111) surface and also depends on the step structure. One of the origins of these behaviors may be that the lattice contraction in the microterrace induced by the step lowers the probability of activated O_2 chemisorption and causes reactivity lower than that of a flat (111) surface.

Acknowledgements

The author acknowledges Professor Ludo Juurlink for his instruction regarding how to prepare a clean, curved Pt(111) crystal surface. This work was supported by JSPS KAKENHI Grant Numbers 20H02623 and 24K01349, as well as the Iketani Science and Technology Foundation.

References

(1) Van Spronsen, M. A.; Frenken, J. W.; Groot, I. M. Surface science under reaction conditions: CO oxidation on Pt and Pd model catalysts. *Chemical Society Reviews* **2017**, *46*, 4347–4374.

(2) Hopster, H.; Ibach, H.; Comsa, G. Catalytic oxidation of carbon monoxide on stepped platinum (111) surfaces. *Journal of Catalysis* **1977**, *46*, 37–48.

(3) Sander, M.; Imbihl, R.; Ertl, G. Kinetic oscillations in catalytic CO oxidation on a cylindrical Pt single crystal surface. *The Journal of Chemical Physics* **1992**, *97*, 5193–5204.

(4) Garcia-Martinez, F.; García-Fernández, C.; Simonovis, J. P.; Hunt, A.; Walter, A.; Waluyo, I.; Bertram, F.; Merte, L. R.; Shipilin, M.; Pfaff, S. et al. Catalytic Oxidation

of CO on a Curved Pt (111) Surface: Simultaneous Ignition at All Facets through a Transient CO-O Complex. *Angewandte Chemie* **2020**, *132*, 20212–20218.

(5) García-Martínez, F.; Rämisch, L.; Ali, K.; Waluyo, I.; Bodero, R. C.; Pfaff, S.; Villar-García, I. J.; Walter, A. L.; Hunt, A.; Pérez-Dieste, V. et al. Structure matters: asymmetric CO oxidation at Rh steps with different atomic packing. *Journal of the American Chemical Society* **2022**, *144*, 15363–15371.

(6) Schiller, F.; Ilyn, M.; Pérez-Dieste, V.; Escudero, C.; Huck-Iriart, C.; Ruiz del Arbol, N.; Hagman, B.; Merte, L. R.; Bertram, F.; Shipilin, M. et al. Catalytic oxidation of carbon monoxide on a curved Pd crystal: spatial variation of active and poisoning phases in stationary conditions. *Journal of the American Chemical Society* **2018**, *140*, 16245–16252.

(7) Blomberg, S.; Zetterberg, J.; Zhou, J.; Merte, L. R.; Gustafson, J.; Shipilin, M.; Trinchero, A.; Miccio, L. A.; Magaña, A.; Ilyn, M. et al. Strain dependent light-off temperature in catalysis revealed by planar laser-induced fluorescence. *ACS Catalysis* **2017**, *7*, 110–114.

(8) Walter, A. L.; Schiller, F.; Corso, M.; Merte, L. R.; Bertram, F.; Lobo-Checa, J.; Shipilin, M.; Gustafson, J.; Lundgren, E.; Brión-Ríos, A. X. et al. X-ray photoemission analysis of clean and carbon monoxide-chemisorbed platinum (111) stepped surfaces using a curved crystal. *Nature communications* **2015**, *6*, 8903.

(9) Roorda, T.; Auras, S. V.; Juurlink, L. B. Chiral Surface Characterisation and Reactivity Toward H–D Exchange of a Curved Platinum Crystal. *Topics in Catalysis* **2020**, *63*, 1558–1568.

(10) Van Lent, R.; Auras, S. V.; Cao, K.; Walsh, A. J.; Gleeson, M. A.; Juurlink, L. B. Site-specific reactivity of molecules with surface defects-the case of H_2 dissociation on Pt. *Science* **2019**, *363*, 155–157.

(11) Cao, K.; van Lent, R.; Kleyn, A. W.; Kurahashi, M.; Juurlink, L. B. Steps on Pt stereodynamically filter sticking of O_2. *Proceedings of the National Academy of Sciences* **2019**, *116*, 13862–13866.

(12) Auras, S. V.; Juurlink, L. B. Recent advances in the use of curved single crystal surfaces. *Progress in Surface Science* **2021**, *96*, 100627.

(13)

(14) Auerbach, D. J.; Tully, J. C.; Wodtke, A. M. Chemical dynamics from the gas-phase to surfaces. *Natural Sciences* **2021**, *1*, e10005.

(15) Kleyn, A. Molecular beams and chemical dynamics at surfaces. *Chemical Society Reviews* **2003**, *32*, 87–95.

(16) Luntz, A.; Williams, M.; Bethune, D. The sticking of O_2 on a Pt (111) surface. *The Journal of Chemical Physics* **1988**, *89*, 4381–4395.

(17) Jacobse, L.; den Dunnen, A.; Juurlink, L. B. The molecular dynamics of adsorption and dissociation of O_2 on Pt (553). *The Journal of Chemical Physics* **2015**, *143*, 014703.

(18) Ueta, H.; Kurahashi, M. Dynamics of O_2 Chemisorption on a Flat Platinum Surface Probed by an Alignment-Controlled O_2 Beam. *Angewandte Chemie International Edition* **2017**, *56*, 4174–4177.

(19) de Willigen, M. J.; Kurahashi, M.; Juurlink, L. B. Alignment and impact angular dependence to O_2 sticking and dissociation on Pt (111) and close-packed steps. *Physical Chemistry Chemical Physics* **2022**, *24*, 18227–18235.

(20) Kurahashi, M.; Yamauchi, Y. Steric effect in O_2 sticking on Al (111): Preference for parallel geometry. *Physical Review Letters* **2013**, *110*, 246102.

(21) Kurahashi, M. Oxygen adsorption on surfaces studied by a spin-and alignment-controlled O_2 beam. *Progress in Surface Science* **2016**, *91*, 29–55.

(22) Kurahashi, M.; Yamauchi, Y. Production of a single spin-rotational state [(J, M)=(2, 2)] selected molecular oxygen ($^3\Sigma_g^-$) beam by a hexapole magnet. *Review of Scientific Instruments* **2009**, *80*, 083103.

(23) King, D. A.; Wells, M. G. Molecular beam investigation of adsorption kinetics on bulk metal targets: Nitrogen on tungsten. *Surface Science* **1972**, *29*, 454–482.

(24) Henzler, M. LEED-investigation of step arrays on cleaved germanium (111) surfaces. *Surface Science* **1970**, *19*, 159–171.

(25) Ueta, H.; Kurahashi, M. Steric effect in CO oxidation on Pt (111). *The Journal of Chemical Physics* **2017**, *147*, 194705.

(26) Burnett, D. J.; Capitano, A. T.; Gabelnick, A. M.; Marsh, A. L.; Fischer, D. A.; Gland, J. L. In-situ soft X-ray studies of CO oxidation on the Pt (111) surface. *Surface Science* **2004**, *564*, 29–37.

(27) Campbell, C.; Ertl, G.; Kuipers, H.; Segner, J. A molecular beam study of the catalytic oxidation of CO on a Pt (111) surface. *The Journal of Chemical Physics* **1980**, *73*, 5862–5873.

(28) Luo, J.; Tobin, R.; Lambert, D. K.; Fisher, G. B.; DiMaggio, C. L. CO adsorption site occupation on Pt (335): a quantitative investigation using TPD and EELS. *Surface Science* **1992**, *274*, 53–62.

(29) Comsa, G.; Mechtersheimer, G.; Poelsema, B. He-beam scattering study of the dynamics of oxygen induced reconstruction of the Pt (997) surface: I. Dynamics of double step formation and destruction. *Surface Science* **1982**, *119*, 159–171.

(30) Hoogers, G.; King, D. Adsorbate-induced step-doubling reconstruction of a vicinal metal surface: oxygen on Rh {332}. *Surface science* **1993**, *286*, 306–316.

(31) Mavrikakis, M.; Hammer, B.; Nørskov, J. K. Effect of strain on the reactivity of metal surfaces. *Physical Review Letters* **1998**, *81*, 2819.

(32) Temmel, S. E.; Fabbri, E.; Pergolesi, D.; Lippert, T.; Schmidt, T. J. Investigating the role of strain toward the oxygen reduction activity on model thin film Pt catalysts. *ACS Catalysis* **2016**, *6*, 7566–7576.

TOC Graphic

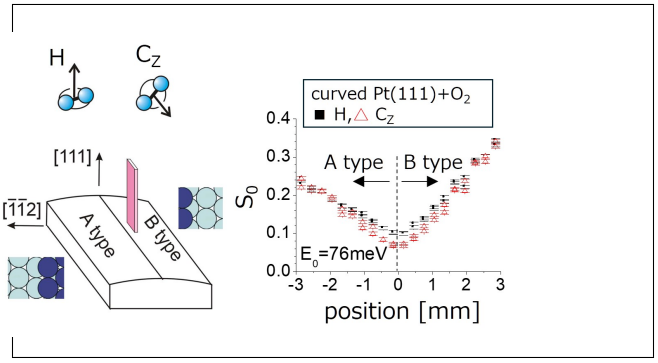
H
C_Z
[111]
[$\bar{1}\bar{1}$2]
A type
B type
curved Pt(111)+O_2
■ H, △ C_Z
A type
B type
S_0
E_0=76meV
0.4
0.3
0.2
0.1
0.0
-3
-2
-1
0
1
2
3
position [mm]